

JOINT INSTITUTE FOR NUCLEAR RESEARCH

Separation of quark and gluon jets using neural network approach in the processes with the direct photon production at the LHC.D.V. Bandourin¹, N.B. Skachkov²*E-mail: (1) dmv@cv.jinr.ru, (2) skachkov@cv.jinr.ru**Laboratory of Nuclear Problems***Abstract**

A neural network technique is used here to discriminate between quark and gluon jets produced in the $qg \rightarrow q + \gamma$ and $q\bar{q} \rightarrow g + \gamma$ processes at the LHC. Considering the network as a trigger and using the PYTHIA event generator and the full event fast simulation package for the CMS detector CMSJET the signal to background ratios are obtained.

1. Introduction.

In the production of a direct photon two QCD processes mainly contribute: the “Compton-like” process

$$qg \rightarrow q + \gamma \quad (1)$$

and the “annihilation” process

$$q\bar{q} \rightarrow g + \gamma. \quad (2)$$

In our paper [1] was proposed to use the direct photon production processes to extract a gluon distribution function in a proton $f^g(x, Q^2)$. It can be done by selection those “ $\gamma + jet$ ” events which satisfy the criteria pointed in papers [2] and [3] to suppress the next-to-leading order diagrams with an initial state radiation and the background to the direct photon from the neutral decay channels of the $\pi^0, \eta, K_s^0, \omega$ —mesons and the photons radiated from a quark in the QCD processes with big cross sections (like $qq \rightarrow qq, q\bar{q} \rightarrow q\bar{q}$ and $qg \rightarrow qg$ scatterings).

It was also shown there a percentage of the “Compton-like” process (1) (amounting to 100% together with (2)) for different $E_t^{jet} (\approx E_t^\gamma)$ and η^{jet} intervals:

Table 1: A percentage of the “Compton-like” process $qg \rightarrow \gamma + q$.

Calorimeter part	E_t^γ interval (GeV)		
	40–50	100–120	200–240
Barrel	89	84	78
Endcap+Forward	86	82	74

In the table above the string “Barrel” corresponds to the Barrel region of the CMS calorimeter ($|\eta| < 1.4$) while the string “Endcap+Forward” corresponds to the Endcap+Forward region ($1.4 < |\eta| < 5.0$).

Thus, an admixture of the processes with a gluon jet in the final state grows from the left upper corner to the right bottom one, i.e. with a jet energy. Therefore, to collect a clean “ $\gamma + quark jet$ ” events sample a necessity of the “ $\gamma + gluon jet$ ” events rejection arises. This necessity is most sharp in the Endcap+Forward region for jets with $E_t^{jet} > 100$ GeV where the part of the “ $\gamma + gluon jet$ ” events is more than 20% and where one can reach the smallest x values of the gluon distribution function $f^g(x, Q^2)$ (see [1]).

The idea of the Artificial Neural Network (ANN) usage for discriminating quarks from gluons was widely discussed in the literature ([4] – [8]). In [7], [8] the discrimination procedure is described for e^+e^- reactions at $\sqrt{s} = 29, 92$ GeV with three different Monte Carlo (MC) generators: JETSET, ARIADNE and HERWIG. After testing with a middle point criterion the network was able to classify

correctly, on the average, 85% of quark and gluon jets for a testing set. The MC independence of the results was also demonstrated by training on the MC data simulated by one generator and by testing on the MC data from another. We also refer to paper [10] where MC independence (JETSET/HERWIG) of the quark/gluon separation procedure basing on the moment analysis of jet particles is presented.

In [5] ANN was applied to a set of $p\bar{p}$ events at $\sqrt{s} = 630\text{ GeV}$ generated with PYTHIA [11]. UA2 calorimeter geometry was used there to classify quark and gluon jets produced in the $qq \rightarrow qq$, $q\bar{q} \rightarrow q\bar{q}$ and $gg \rightarrow gg$ QCD subprocesses only. The 70 – 72% classification ability with respect to the middle point criterion was reached there. In this paper we apply the ANN approach to get the most effective discrimination of quark and gluon jets in the processes (1) and (2) selected by the cuts given in Section 4 and in [2], [3].

The study was carried out using the JETNET 3.0 package ¹ developed at CERN and the University of Lund [4].

2. Artificial Neural Network.²

2.1 General description.

It was well established that the basic unit of signal processing in the brain is *a neuron*. There are about 10^{11} inter-connected neurons in a human brain, each of which has essentially the same structure. The signals arriving at a neuron are summed and if this sum is greater than some threshold, the neuron is “fired”. After firing the neuron returns back to its initial state. The signals are electrical pulses caused by biochemical changes. The fired neuron in turn sends a signal to the connected neurons which may result in the firing of the other neuron in the network. The key feature of the process is the linear summations of inputs and non-linear transformation of the sum.

Artificial Neural Networks are mathematical models that are inspired by the connections and the functionality of neurons in biological system. They have given rise to a branch of research called neural computing which has application in many disciplines. The basic concept is based on two ideas: the topology of nodes/connections and transfer functions which relate the input and output of each node.

ANN is often used as a way of optimizing a classification (or pattern recognition) procedure and have been applied to many pattern recognition problems in high energy physics (see [5] – [8], [9], [16], [17]) with a notable success. They usually have more input than output nodes and thus may be viewed as a performing of dimensionality reduction of input data set.

¹It is available via *anonymous* ftp from thep.lu.se or from freehep.scri.fsu.edu.

²This section is based mainly on the material of papers [4] and [9].

ANN approach is a technique which assigns objects to various classes. These objects can be different data types such as signal and background in our case. Each data type is assigned to a class which in the context of the given paper is 0 for background (gluon jet) and 1 for signal (quark jet). Discrimination is achieved by looking at the class to which the data belongs. The technique fully exploits the correlation among different variables and provides a discriminating boundary between the signal and background.

ANN's have an ability to learn, remember and create relationships amongst the data. There are many different types of ANN but the feed forward types are most popular in the high energy physics. Feed forward implies that information can only flow in one direction and output determines directly the probability that an event characterized by some input pattern vector $X(x_1, x_2, \dots x_n)$ is from the signal class.

2.2 A mathematical model of the neural network.

The mathematical model of the Neural Network (NN) reflects the three basic functions of a biological neuron:

- sum up all the information arriving at inputs of node/neuron;
- if sum is greater than some threshold, fire neuron;
- after firing, return to the initial state and send a signal to each of the other neighbouring neurons in the network.

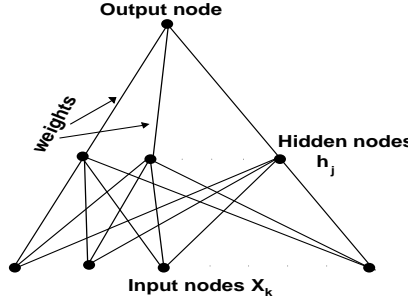


Fig. 1: Neural network with one layer of hidden units.

The neuron with these characteristics is known as an elementary perceptron. The perceptron is a simple feed forward system with several input connections and a single output connection. Mathematically output can be written as:

$$O(x_1, x_2, \dots x_n) = g\left(\frac{1}{T} \sum_i \omega_i x_i + \theta\right). \quad (3)$$

Here g is a non-linear transfer function and typically takes the following form (sigmoid function):

$$g = \frac{1}{1 + e^{-2x}} \quad (4)$$

(x_1, x_2, \dots, x_n) is the input pattern vector, O is the output, ω_i and θ are independent parameters called weights (which connect the input nodes to the output node) and a threshold of the output node respectively. $\beta = 1/T$ is called inverse temperature and defines the slope of g .

A pattern vector x_i is multiplied by the connection weights ω_i so that each piece of information appears at the perceptron as $\omega_i x_i$. Then the perceptron sums all the incoming information to give $\sum \omega_i x_i$ and applies the transfer function g to give the output (see (3)).

In a feed forward NN a set of neurons has a layered structure. Fig. 1 shows the feed forward NN with one hidden layer that is used here. In this case the output of NN is:

$$O(x_1, x_2, \dots, x_n) = g\left(\frac{1}{T} \omega_j \sum_k g\left(\frac{1}{T} \sum_k \omega_{jk} x_k + \theta_j\right) + \theta\right), \quad (5)$$

where ω_{jk} are the weight connecting input node k to hidden node j and ω_j 's connect the hidden nodes to the output node. θ_j and θ are thresholds of the hidden and output node respectively.

3. Learning of the perceptron.

The behaviour of a perceptron is determined by independent parameters known as weights and thresholds. The totalt number of independent parameters in a neural network with a single layer is given by:

$$N_{ind} = (N_{in} + N_{on}) \cdot N_{hn} + N_{ht} + N_{ot} \quad (6)$$

where N_{in} is a number of input nodes, N_{on} is a number of output nodes, N_{hn} is a number of nodes in a hidden single layer, N_{ht} is a number of thresholds in a hidden single layer, N_{ot} is a number of output thresholds.

Learning is the process of adjusting these N_{ind} parameters. During learning to every perceptron are shown examples of what it must learn to interpret. It is fulfilled on the training set consisting of two parts: the training data (a collection of input patterns to the perceptron) and the training target what is a desired output of each pattern.

Mathematically, the goal of training is to minimize a measure of the error. The mean squared error function E averaged over the training sample is defined by equation (7):

$$E = \frac{1}{2N_p} \sum_{p=1}^{N_p} \sum_{i=1}^N (O_i^{(p)} - t_i^{(p)})^2, \quad (7)$$

where O_i is the output of i -th node of NN in equation (5); t_i is the training target (in our case, 0 for background and 1 for signal); N_p is a number of patterns (events) in the training sample; N is number of the network outputs ($N = 1$ for our case).

There are several algorithms for error minimization and weights updating. Most popular are **Back propagation**, **Langevin** and **Manhattan** methods. In the last one the weight is updated during the learning by the following rule ³:

$$\omega_{t+1} = \omega_t + \Delta\omega \quad (8)$$

$$\Delta\omega = -\eta \cdot \text{sgn}[\partial E / \partial \omega] \quad (9)$$

where ω is the vector of weights and thresholds used in the network; t ($t + 1$) refers to the previous (current) training cycle and η is the learning rate which is decreased in the learning process.

4. Events selection and Monte Carlo simulations for the ANN analysis.

Our selection conditions for the “ $\gamma + jet$ ” events are based on the selection rules chosen in [2] and [3]. We suppose the electromagnetic calorimeter (ECAL) size to be limited by $|\eta| \leq 2.61$ and hadronic calorimeter (HCAL) is limited by $|\eta| \leq 5.0$ (the CMS geometry; see [13] and [14]) where $\eta = -\ln(\tan(\theta/2))$ is a pseudorapidity defined through a polar angle θ counted from the beam line. In the plane transverse to the beam line the azimuthal angle ϕ defines the directions of \vec{E}_t^{jet} and \vec{E}_t^γ .

1. We select the events with one jet and one photon candidate with

$$E_t^\gamma \geq 40 \text{ GeV}, \quad E_t^{jet} \geq 30 \text{ GeV}. \quad (10)$$

A jet is defined here according to the PYTHIA jetfinding algorithm LUCCELL ⁴. The jet cone radius R in the $\eta - \phi$ space is taken as $R = ((\Delta\eta)^2 + (\Delta\phi)^2)^{1/2} = 0.7$.

2. Only the events with “isolated” photons are taken to suppress the background processes. To do this, we restrict:

a) the value of the scalar sum of E_t of hadrons and other particles surrounding a photon within a cone of $R_{isol}^\gamma = ((\Delta\eta)^2 + (\Delta\phi)^2)^{1/2} = 0.7$ (“absolute isolation cut”)

$$\sum_{i \in R} E_t^i \equiv E_t^{isol} \leq E_{tCUT}^{isol}; \quad (11)$$

b) the value of a fraction (“relative isolation cut”)

$$\sum_{i \in R} E_t^i / E_t^\gamma \equiv \epsilon_{CUT}^\gamma \leq \epsilon_{CUT}^\gamma; \quad (12)$$

c) we accept only the events having no charged tracks (particles) with $E_t > 1 \text{ GeV}$ within the R_{isol}^γ cone around a photon candidate.

3. We consider the structure of every event with the photon candidate at a more precise level of the 5×5 crystal cells window (size of one CMS HCAL tower) with

³see [6] for a more complete description

⁴the PYTHIA’s default jetfinding algorithm

a cell size of 0.0175×0.0175 . To suppress the background events with the photons resulting from high energetic π^0 , η , ω and K_S^0 mesons we require ⁵:

a1) the absence of a high E_t hadron in this 5×5 crystal cell window (at the PYTHIA level of simulation):

$$E_t^{hadr} \leq 5 \text{ GeV}. \quad (13)$$

a2) the transverse energy deposited in HCAL in the radius $R = 0.7$ counted from the center of gravity of HCAL tower just behind the ECAL 5×5 window, containing a direct photon signal, to be limited by (at the level of the full event simulation; see below) :

$$E_t^{HCAL} \leq 1 \text{ GeV}. \quad (14)$$

4. The events with the vector \vec{E}_t^{jet} being “back-to-back” to the vector \vec{E}_t^γ in the transverse to a beam line plane within $\Delta\phi$ which is defined by equation:

$$\phi_{(\gamma,jet)} = 180^\circ \pm \Delta\phi \quad (\Delta\phi = 15^\circ, 10^\circ, 5^\circ) \quad (15)$$

(5° is a size of one CMS HCAL tower in ϕ) for the following definition of the angle $\phi_{(\gamma,jet)}$: $\vec{E}_t^\gamma \vec{E}_t^{jet} = E_t^\gamma E_t^{jet} \cdot \cos(\phi_{(\gamma,jet)})$, with $E_t^\gamma = |\vec{E}_t^\gamma|$, $E_t^{jet} = |\vec{E}_t^{jet}|$.

5. To discard additionally the background events, we choose only the events that do not have any other (except one jet) minijet-like or cluster high E_t activity with the E_t^{clust} higher than some threshold E_{tCUT}^{clust} value. Thus we select events with

$$E_t^{clust} \leq E_{tCUT}^{clust}, \quad (16)$$

where clusters are found by the same jetfinder LUCELL used to find a jet in the same event.

The following values of cut parameters were used here:

$$E_{tCUT}^{isol} = 5 \text{ GeV}; \quad \epsilon_{CUT}^\gamma = 7\%; \quad \Delta\phi < 15^\circ; \quad E_{tCUT}^{clust} = 10 \text{ GeV}. \quad (17)$$

To obtain results of this paper two types of the generations were done:

- (a) by using PYTHIA only and basing on the averaged calorimeter cells sizes $\Delta\eta \times \Delta\phi$: 0.087×0.087 in the Barrel, 0.134×0.174 in the Endcap and 0.167×0.174 in the Forward parts;
- (b) by using CMSJET – the full event fast Monte Carlo simulation package of a response in the CMS detector [12] with the switched on calorimeter and magnetic field effects.

The following E_t^γ intervals were considered for the both types of generations (a) and (b) (see above): $40 < E_t^\gamma < 50$, $100 < E_t^\gamma < 120$, $200 < E_t^\gamma < 240 \text{ GeV}$.

⁵At the PYTHIA level of simulation this cut may effectively take into account the imposing of an upper cut on the HCAL signal in the tower behind the ECAL 5×5 crystal cells window hit by the direct photon (see [18]).

Besides, for every E_t interval we separates the regions to which jet belongs: Barrel and Endcap+Forward. Since the jet is a spatially spread object, some energy leakage from one calorimeter part to another is possible. To distinguish cases when a jet in the Barrel or in the Endcap+Forward regions the following restriction was added to the cuts 1–5:

$$\Delta E_t^{jet}/E_t^{jet} = 0 \text{ -- for the PYTHIA level study; } \quad (18)$$

$$\Delta E_t^{jet}/E_t^{jet} \leq 0.05 \text{ -- for the CMSJET level study. } \quad (19)$$

Here ΔE_t^{jet} is the jet E_t leakage from that part of the calorimeter in which the jet gravity center was found.

5. Training and testing of ANN.

There are two stages in the neural network analysis. The first is training of the network and the second is testing. NN is trained on samples of signal and background events and tested using independent data sets. Training the network corresponds to step-by-step changing the weights ω_{jk} such that a given input vector $X^{(p)}(x_1, x_2, \dots, x_n)$ produces an output value $O^{(p)}$ that equals the desired output or target value $t^{(p)}$ (see (5) and (7)).

The input parameters used in the 0-th (input) layer of the network (Fig. 1) were chosen as follows. In “Set 01” and “Set 02” we have analyzed the jet information obtained in PYTHIA’s simulation. In Set 01 we assign E_t , η and ϕ of the first E_t leading cell to the nodes x_1 , x_2 and x_3 correspondingly. Then we take second leading cell and assign its E_t , η and ϕ to x_4 , x_5 and x_6 nodes. The same we do for the remaining 13 cells. So, we have 45 input nodes in total ⁶. In Set 02 we add 46-th input node with a number of charged tracks N_{track} inside a jet with $E_t^{ch} > 1 \text{ GeV}$. For “Set 1” and “Set 2” we repeat previous procedure but with respect to the cells of jets found after the fast Monte Carlo simulation of the whole event using CMSJET. Analogously we have 45 and 46 ($+N_{track}$ information) nodes for Sets 1 and 2.

To ensure convergence and stability, the total number of training patterns (events) must be significantly larger (20-30 times) than the number of independent parameters (see (6)). By 7000 of signal (with a quark jet) and background (with a gluon jet) events were chosen for the training stage, i.e. about 30 patterns per a weight.

After NN has been trained, a test procedure is implemented in which the events not used in training were passed through the network. The same proportion of the signal and background events (by 7000 of each sort) was used at the generalization stage. An output is provided for each event and can be considered as a probability that an event is either from signal or background sample. If the training has been done correctly, the probability for an event being signal is high if the output O is

⁶This input set is the same as in paper [5]. It was checked out that variations to 10 or to 20 cells data on the input do not much effect the result.

close to 1. And conversely if the output O is close to 0 then it is more likely to be a background event (see Fig. 2 for the case of jets found in the Endcap+Forward region and $40 < E_t^\gamma < 50 \text{ GeV}$ as an example of a typical NN output).

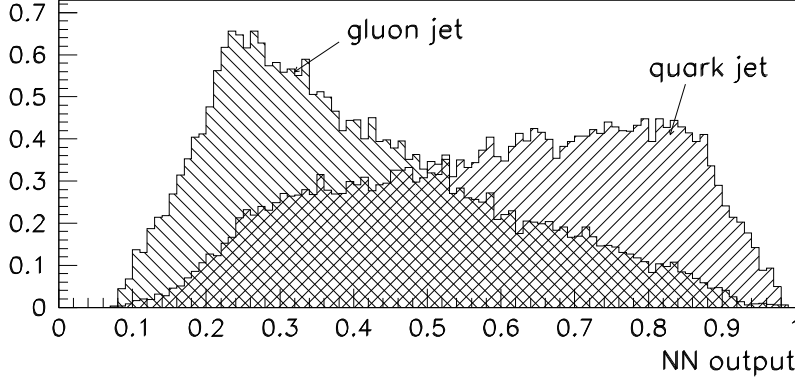


Fig. 2: Neural network output for quark and gluon jets in the Endcap+Forward region, $40 < E_t^\gamma < 50 \text{ GeV}$.

6. The choice of neural network architecture and learning parameters.

To investigate a dependence on the learning parameters, we trained a neural network with 7000 signal events and 7000 background events found after the CMSJET simulation. In those events the direct photon E_t was chosen to be $100 < E_t^\gamma < 120 \text{ GeV}$ and jets were found in the Barrel region.

Than the network was tested with independent set of 7000 signal and background events. A sensitivity to different NN parameters were tested from the point of view of NN quark/gluon separation probability with respect to the “0.5-criterion” criterion (point 0.5 of the NN output). These parameters are itemized below and corresponding plots are given in Figs. 3 and 4.

- *Number of training cycles*

We varied number of training cycles from 100 to 1000 to investigate the effect of training on the network performance. The result shown in Fig. 3 indicates the network stability if more than training cycles are used.

- *Inverse temperature*

The inverse temperature determines the steepness of the transfer function $g(x)$ (4). On the left-hand upper plot of Fig. 4 the quark/gluon separation probability drops by 1% while moving from $\beta = 0.5 - 1$ to $\beta = 1.5 - 1.8$.

- *Number of hidden nodes*

One hidden layer is used here because it is sufficient for most classification problems [4]. Sensitivity of the quark/gluon separation probability to a number

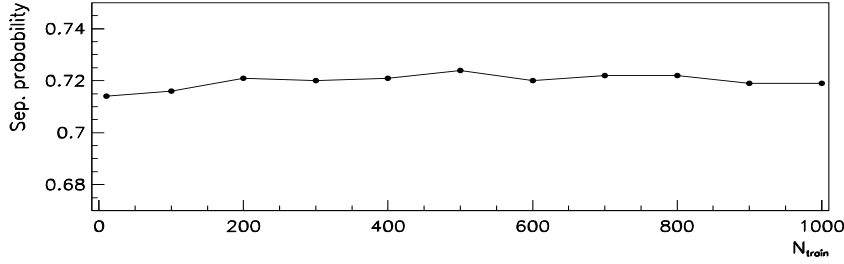


Fig. 3: The quark/gluon separation probability using “0.5-criterion” as a function of the number of training cycles N_{train} .

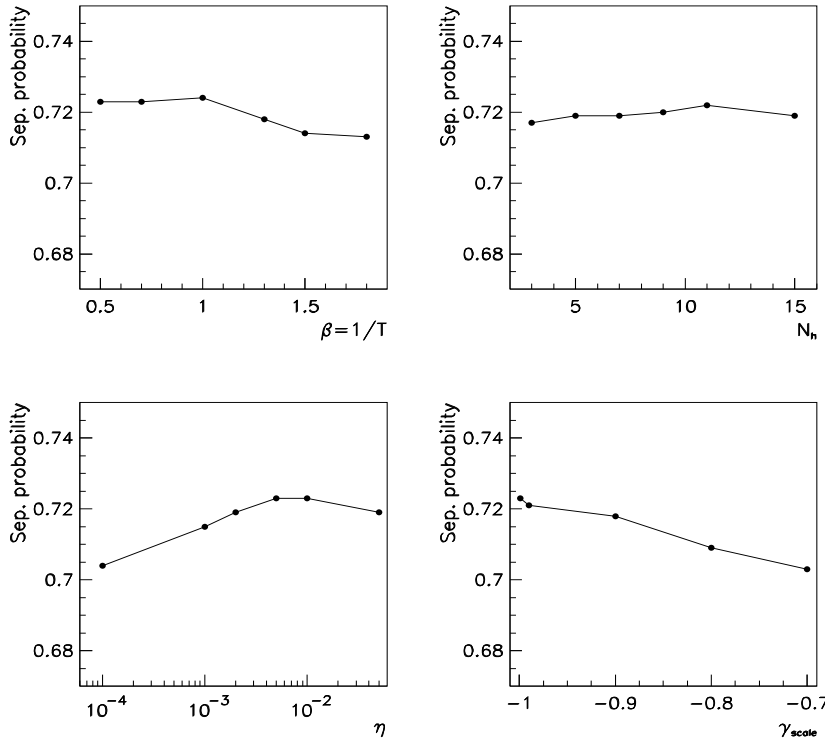


Fig. 4: The quark/gluon separation probability using the “0.5-criterion” criterion for various network parameters: inverse temperature $\beta = 1/T$, number of hidden nodes N_h , learning rate η , η updating scale parameter γ_{scale} .

of hidden nodes N_h was tested with $N_h = 3 - 15$. All resulting points are comprised within 1% (71 – 72%) window (see Fig. 4)⁷.

- *Learning rate η*

Learning rate η is a factor in updating the weights. We varied its value between 0.0001 and 0.05 (see left-hand bottom plot in Fig. 4). The value $\eta = 0.005$ for our analysis was chosen.

- *Scale parameter γ_{scale}*

The optimal learning rate η varies during learning while the network converges towards the solution. The scale factor for its changing is determined by γ_{scale} parameter. The right-hand bottom plot in Fig. 4 shows that optimal performance is achieved at default value $\gamma_{scale} = -1$.

As it was mentioned above, the Manhattan updating method was used here during training procedure. In Table 2 for the case of jets in the Barrel region and $100 < E_t^\gamma < 120 \text{ GeV}$ (Set 2) is briefly presented a comparison with other updating algorithms with various values of learning parameters: learning rate η (Backpropagation, Langevin) and noise term σ (Langevin). It is seen that varying η and σ from their default values in the JETNET package (the first column for each algorithm) one can approximately reach the value of the separation probability obtained by using Manhattan algorithm (72%).

Table 2: A dependence of the separation probability (%) using “0.5-criterion” on the method. CMSJET, Set 2, Barrel region, $100 < E_t^\gamma < 120 \text{ GeV}$.

Method	Backpropagation			Langevin		
	$\eta = 1.$	$\eta = 0.5$	$\eta = 0.1 - 0.001$	$\eta = 1.0$	$\eta = 0.1 - 0.01$	$\eta = 0.01$
Parameters				$\sigma = 0.01$	$\sigma = 0.01$	$\sigma = 0.001$
Probab. (%)	51	68	71	69	70	71

7. Results description.

The discrimination powers for different sets of incoming data with respect to the middle point success criterion are presented in Tables 3 and 4 for three various intervals of the direct photon E_t . The 1 – 3% growth of the separation probability after introducing the information on the number of tracks N_{track} in the Barrel region is seen. The analogous increase for the Endcap+Forward region is 3 – 6% at the PYTHIA level and 1 – 3% at the level of the full event simulation with CMSJET.

To give an understanding of such an improvement we plot, as an example, a distribution of the number of events over N_{track} for $40 < E_t^\gamma < 50 \text{ GeV}$ and $200 < E_t^\gamma < 240 \text{ GeV}$ in the Barrel region (Fig. 5). Due to the larger bremsstrahlung probability from a gluon as compared with a quark we obtain the $\langle N_{track}^g \rangle / \langle N_{track}^q \rangle$

⁷To be exact, a bit better result is achieved with $N_h = 11$.

Table 3: The quark/gluon separation probability (%) using “0.5-criteria”. Barrel region.

Simulation type	Set No.	E_t^γ interval (GeV)		
		40 – 50	100 – 120	200 – 240
PYTHIA	01	74	76	79
	02	75	77	82
CMSJET	1	70	70	71
	2	71	72	73

The error is of order of 1.5 – 2% for all numbers.

Table 4: The quark/gluon separation probability (%) using “0.5-criteria”. Endcap +Forward region

Simulation type	Set No.	E_t^γ interval (GeV)		
		40 – 50	100 – 120	200 – 240
PYTHIA	01	70	69	69
	02	73	74	75
CMSJET	1	68	67	68
	2	69	70	71

The error is of order of 1.5 – 2% for all numbers.

ratio equal to 1.27 for $40 < E_t^\gamma < 50$ GeV and 1.46 for $200 < E_t^\gamma < 240$ GeV.

Figs. 6 – 8 also explain the choice of the variables on the input to NN. As it is seen from Figs. 6 and 7, E_t of the leading cell (“ E_{t1} ” on the plots) in a quark jet is greater by 25 – 30% than in a gluon jet, on the average. The difference in E_t for the next-to-leading cells (“ E_{t2} ” on the plots) in quark and gluon jets is about 10 – 20%

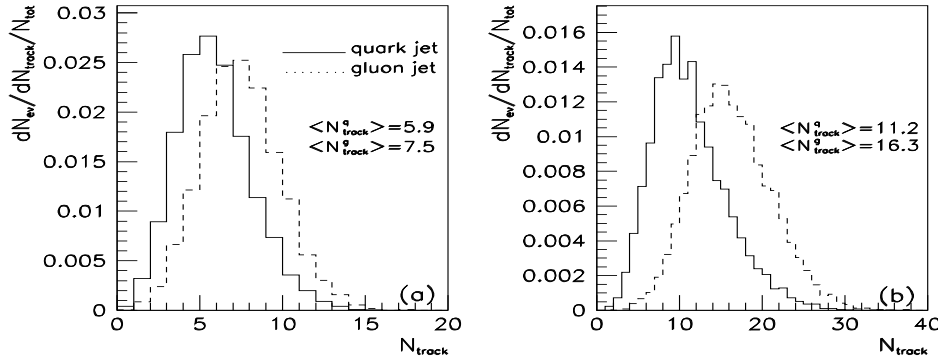


Fig. 5: Distribution over the number of charged tracks with $E_t^{ch} > 1$ GeV for jets found in the Endcap+Forward region: $40 < E_t^\gamma < 50$ GeV (a) and $200 < E_t^\gamma < 240$ GeV (b).

(it is smaller for jets with a higher E_t). E_t of a complete quark jet is also greater than E_t of a complete gluon jet (by 4 – 10%). Again the difference is smaller with a jet E_t growing.

Fig. 8 shows a distribution of the averaged E_t in quark and gluon jets over the distance from the leading cell R_{-ic} for all E_t^γ intervals and calorimeter regions considered in this paper. One can note that in all cases the averaged E_t in a quark jet up to $R_{-ic} \approx 0.12 - 0.14$ is greater than in a gluon jet and, vice versa, averaged E_t in a quark jet for $R_{-ic} \geq 0.14$ is lower than in a gluon jet.

So, using “0.5-criterion” for the ANN output, when the output node value $O > 0.5$ is interpreted as a quark jet and $O < 0.5$ as a gluon jet, the network correctly classifies 75 – 81% (73 – 75%) of jets at the PYTHIA level and 71 – 73% (69 – 71%) at the CMSJET level in the Barrel (Endcap+Forward) region with 45+1 input nodes.

It is also interesting to investigate the Signal/Background ratio as a function of the NN output. This analysis was done after full event simulation using CMSJET for 45+1 input nodes. The corresponding numbers for three E_t^γ intervals and two calorimeter regions is given in Table 5. As a complement to Table 5 we show in Fig. 10 the quark selection and gluon rejection efficiencies in the case of the full simulation for the same E_t^γ intervals and calorimeter regions.

Table 5: Signal/Background. Full simulation using CMSJET. Set 2.

E_t^γ (GeV)	Region	NN output cut					
		0.3	0.4	0.5	0.6	0.7	0.8
40 – 50	Barrel	1.45	1.91	2.40	3.11	4.19	6.16
	Endcap+Forward	1.41	1.81	2.38	3.10	4.04	5.85
100 – 120	Barrel	1.72	2.63	3.26	4.04	4.59	6.37
	Endcap+Forward	1.75	2.19	2.95	3.61	4.21	5.41
200 – 240	Barrel	1.76	2.37	3.35	4.26	5.56	7.36
	Endcap+Forward	1.64	2.40	3.17	4.16	5.39	7.45

The Signal/Background ratio grows as by growing the NN output value as by increasing E_t^γ value (see Table 5). So, it grows as 2.4 to 3.2 at the NN output cut $O > 0.5$ and as 4.0 to 5.4 at $O > 0.7$ for the Endcap+Forward region. The curves on Fig. 10 show that for the last cut ($O > 0.7$) about 38% and 44% of the events with quark jet for $40 < E_t^\gamma < 50$ GeV and $200 < E_t^\gamma < 240$ GeV, respectively, are selected, while about 66 – 67% of the events with quark jet are selected at $O > 0.5$ for the both E_t^γ intervals and the same calorimeter region.

The Signal/Background ratio dependence on the NN output cut at the PYTHIA level is presented in Figs. 12 and 13.

A dependence of the Signal/Background ratio on the quark jet selection efficiency is plotted in Fig. 11 for two utmost considered in this paper E_t^γ intervals and

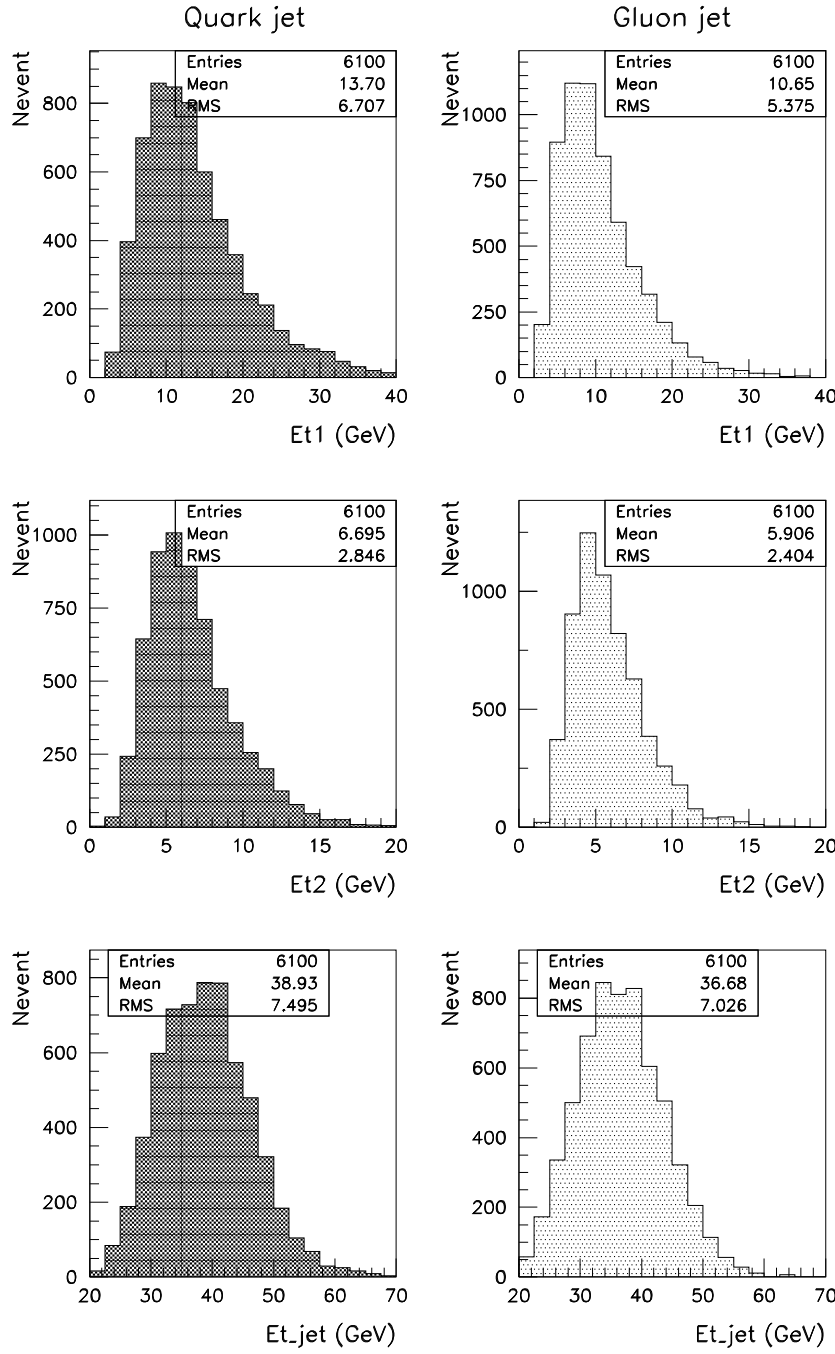


Fig. 6: Distribution over E_t of leading cell ($E_t 1$), E_t of next-to-leading cell ($E_t 2$) and E_t of the full quark and gluon jets. CMSJET, Endcap+Forward, $40 < E_t^\gamma < 50$ GeV

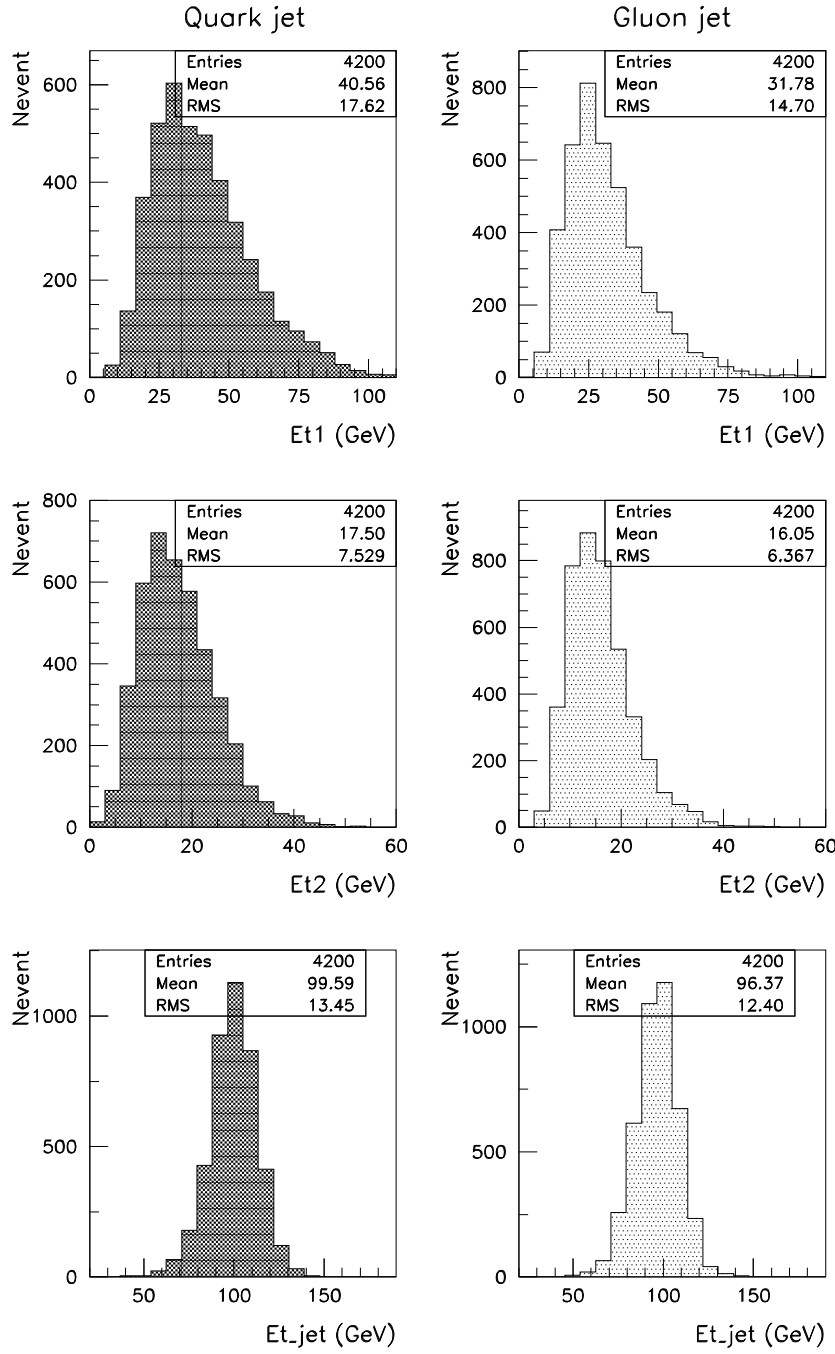


Fig. 7: Distribution over Et of leading cell (E_{t1}), Et of next-to-leading cell (E_{t2}) and Et of the full quark and gluon jets. CMSJET, Endcap+Forward, $100 < E_t \gamma < 120$ GeV

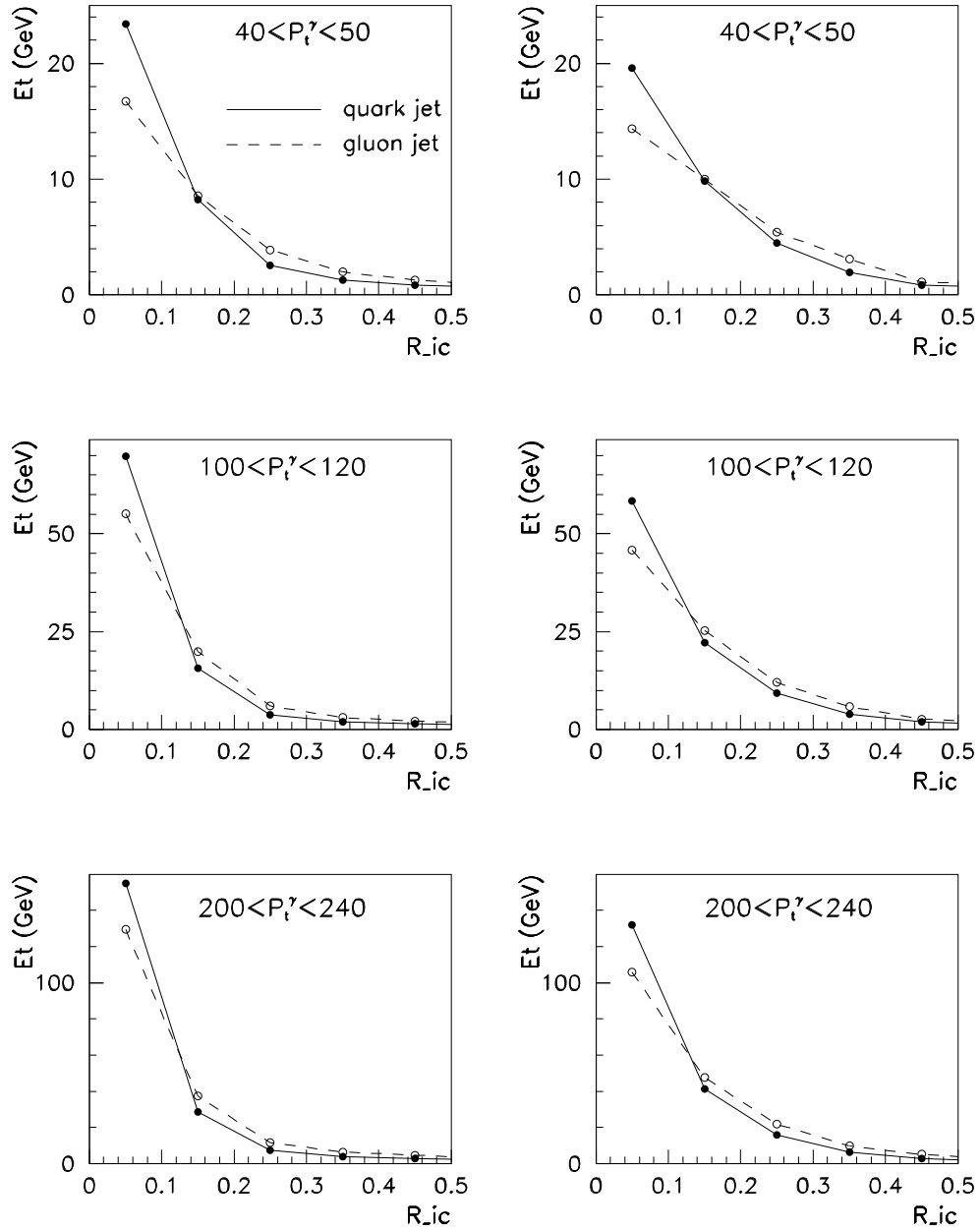


Fig. 8: Distribution of E_t over the distance in the $\eta - \phi$ space from initiator cell inside quark (solid line) and gluon (dashed line) jets. The lefthand column corresponds to the Barrel region and the righthand – to the Endcap+Forward region.

two calorimeter regions. We present there two curves obtained with Set 1 and Set 2 of input information after the full CMSJET event simulation (the thin and thick solid lines) and one curve (dotted line) obtained with Set 02 after event simulation at the PYTHIA level.

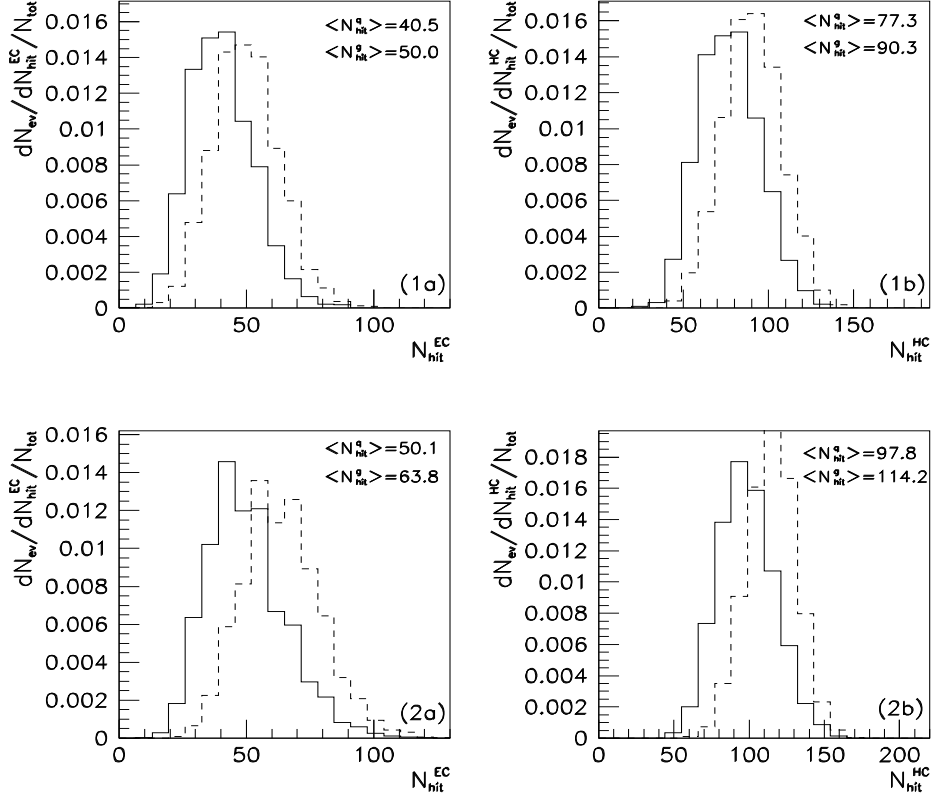


Fig. 9: Distribution over the number of ECAL (plots 1a and 2a) and HCAL cells (plots 1b and 2b) for jets found in the Barrel region: $40 < E_t^\gamma < 50 \text{ GeV}$ (1a, 1b) and $200 < E_t^\gamma < 240 \text{ GeV}$ (1b, 2b).

The results obtained with quark and gluon jets found in the CMSJET simulation were compared with the results obtained after passing quark and gluon jet particles through electromagnetic (ECAL) and hadronic (HCAL) calorimeters in the CMSIM package [15]. The discrimination probabilities received after cells analysis in CMSIM are in fine agreement (up to 1%) with those in Tables 3 for CMSJET. It was also found as in CMSET as in CMSIM that almost the same discrimination powers can be achieved (up to 1 – 2%) by using input information to the network about E_t of the first, ordered by E_t , 15 ECAL and 15 HCAL cells (i.e. 30 input nodes) instead of 45 input nodes as considered above.

It is also interesting to note the sensitivity of the network to some parameters. So, the network is able to classify correctly quark and gluon jets with respect

to the “0.5-criterion” criterion in 65% (67%) of events with $40 < E_t^\gamma < 50 \text{ GeV}$ ($200 < E_t^\gamma < 240 \text{ GeV}$) by using N_{track} variable only. These numbers can be improved by 2 – 3% if we also add to N_{track} other two input variables: the number of activated cells (towers) in ECAL and HCAL belonging to quark and gluon jets. The distributions over those numbers are shown in Fig. 9 for two E_t^γ intervals: $40 < E_t^\gamma < 50 \text{ GeV}$ and $200 < E_t^\gamma < 240 \text{ GeV}$. We see that mean value of the activated cells number in ECAL for the case of gluon jets $\langle N_{hit}^g \rangle$ exceeds that for the case of quark jets $\langle N_{hit}^q \rangle$ by factor of 1.25 for the $40 < E_t^\gamma < 50 \text{ GeV}$ interval. This difference grows up to the factor of 1.67 for the $200 < E_t^\gamma < 240 \text{ GeV}$ interval. And in both intervals the ratio of mean values of the activated cells number $\langle N_{hit}^g \rangle / \langle N_{hit}^q \rangle$ in HCAL is about 1.16 – 1.17.

8. Acknowledgements.

We are greatly thankful to George Gogiberidze (JINR, Dubna) for the helpful discussions on some ideas and methods of the artificial neural network usage for pattern recognition tasks.

References

- [1] D.V. Bandourin, V.F. Konoplyanikov, N.B. Skachkov. “ $\gamma + jet$ ” events rate estimation for gluon distribution determination at LHC”, Part.Nucl.Lett.103:34-43,2000, hep-ex 0011015.
- [2] D.V. Bandourin, V.F. Konoplyanikov, N.B. Skachkov. “Jet energy scale setting with “ $\gamma + jet$ ” events at LHC energies. Generalities, Selection rules”, JINR Preprint E2-2000-251, JINR, Dubna, hep-ex 0011012.
- [3] D.V. Bandourin, V.F. Konoplyanikov, N.B. Skachkov. “Jet energy scale setting with “ $\gamma + jet$ ” events at LHC energies. Detailed study of the background suppression.” JINR Preprint E2-2000-255, JINR, Dubna, hep-ex/0011017.
- [4] C. Peterson, T. Rognvaldsson and L Lonnblad, “JETNET 3.0. A versatile Artificial Neural Network Package”, Lund University Preprint LU-TP 93-29.
- [5] P. Bhat *et al*, “Using Neural Networks to identify jets in hadron-hadron collisions”, DESY Note DESY 90-144, Lund University Preprint LU-TP 90-13.
- [6] Proc. of CERN School of Computing, 1991, Ystad, Sweden, CERN 92-02, p.113 – 170.
- [7] L. Lonnblad C. Peterson and T. Rognvaldsson, “Finding gluon jets with a neural trigger”, Phys.Rev.Lett, **65**, p. 1321 – 1324, 1990.
- [8] L. Lonnblad C. Peterson and T. Rognvaldsson, “Using neural network to identify jets”, Nucl.Phys. **B 349**, p. 675, 1991.

- [9] Harpreet Singh, The measurement of $t\bar{t}$ production cross section in $p\bar{p}$ collision at $\sqrt{s} = 1.8 \text{ TeV}$ using neural network. The PhD thesis, University of California, 1999.
- [10] S. Kanda, S. Kim and K. Kondo, “Moment analysis of charged fragment distributions and separation of quark and gluon jets”. *Comp.Phys.Comm.* **67** (1991)223 – 232.
- [11] T. Sjostrand, *Comp.Phys.Comm.* **82** (1994)74.
- [12] S. Abdullin, A. Khanov, N. Stepanov, CMS Note CMS TN/94–180 “CMSJET”. Version 4.703 was used.
- [13] CMS Electromagnetic Calorimeter Project, Technical Design Report, CERN/LHCC 97–33, CMS TDR 4, CERN, 1997.
- [14] CMS Hadron Calorimeter Project, Technical Design Report, CERN/LHCC 97–31, CMS TDR 2, CERN, 1997.
- [15] GEANT-3 based simulation package of CMS detector, CMSIM, Version 116. CMS TN/93-63, C. Charlot *et al.*, “CMSIM–CMANA. CMS Simulation facilities”, CMSIM User’s Guide at WWW: <http://cmsdoc.cern.ch/cmsim/cmsim.html>.
- [16] L. Borissov, A. Kirkby, H. Newman, S. Shevchenko, CMS Note 1997/050, “Neutral pion rejection in the CMS $PbWO_4$ crystal calorimeter using a neural network”
- [17] A. Kyriakis, D. Loukas, J. Mousa, D. Barney, CMS Note 1998/088, “Artificial neural net approach to $\gamma - \pi^0$ discrimination using CMS Endcap Preshower”.
- [18] D.V. Bandourin, V.F. Konoplyanikov, N.B. Skachkov, “ $\pi^0, \eta, \omega, K_s^0$ mesons and a photon discrimination based on the calorimeter information in the CMS detector”, JINR Preprint in preparation, hep-exp/0108050.

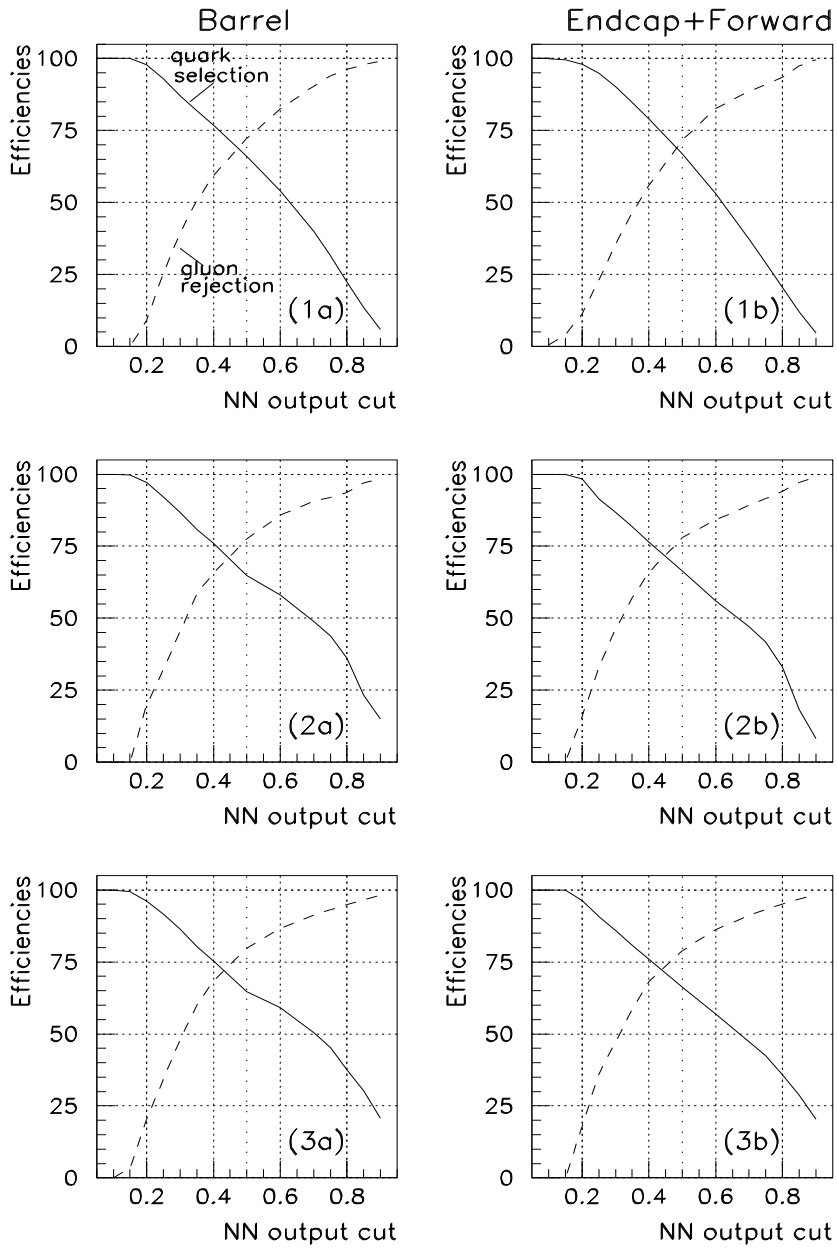


Fig. 10: Quark jet selection and gluon jet rejection efficiencies as a function of neural network output cut. Left-hand (1a, 2a, 3a) and right-hand (1b, 2b, 3b) columns correspond to the Barrel region and to the Endcap+Forward regions. The first row plots (1a, 1b) are for $40 < E_t^\gamma < 50 \text{ GeV}$, the second (2a, 2b) for $100 < E_t^\gamma < 120 \text{ GeV}$ and the third (3a, 3b) for $200 < E_t^\gamma < 240 \text{ GeV}$ intervals.

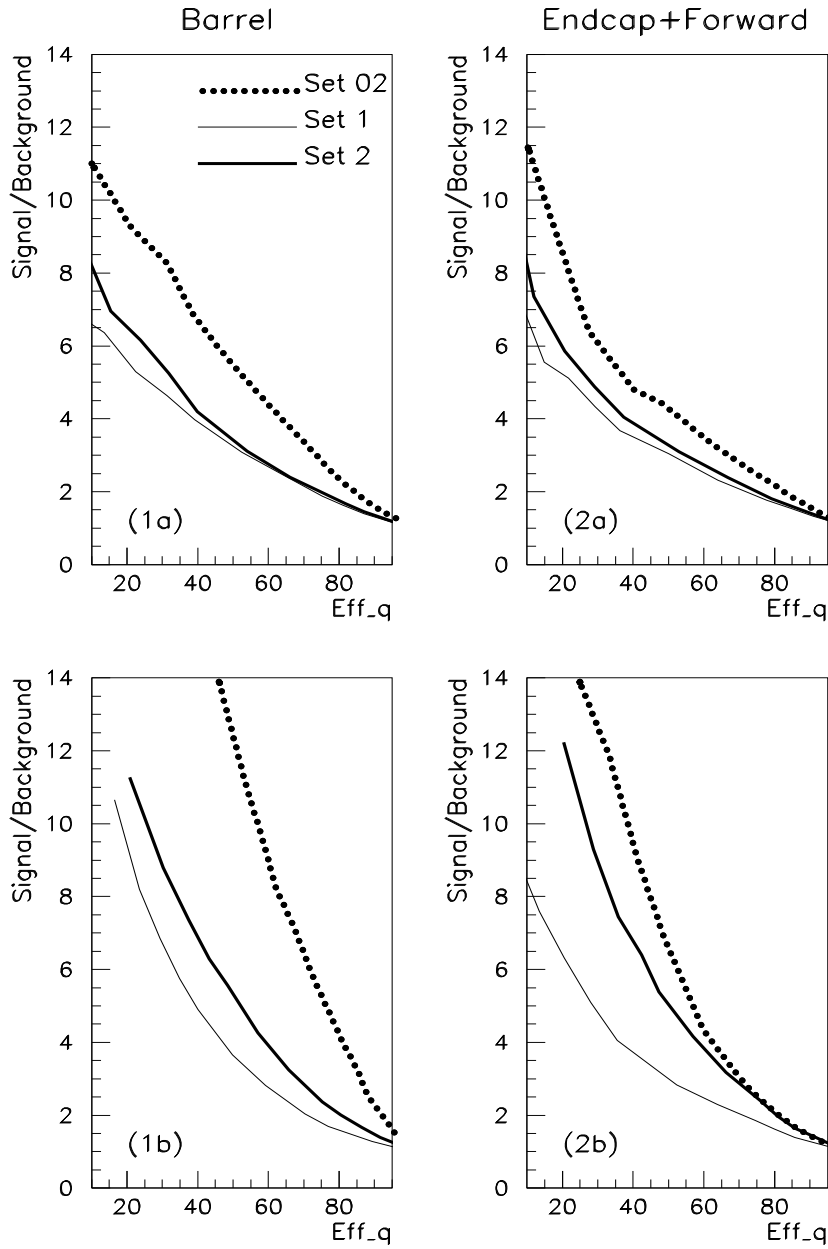


Fig. 11: Signal to background ratio via quark jet selection efficiency. The lefthand column (1a, 2a) correspond to the events with jets found in the Barrel and the righthand (1b, 2b) correspond to the events with jets found in the Endcap+Forward region. In the first row (1a, 2a) are events with $40 < E_t^\gamma < 50 \text{ GeV}$ and in the second with $200 < E_t^\gamma < 240 \text{ GeV}$.

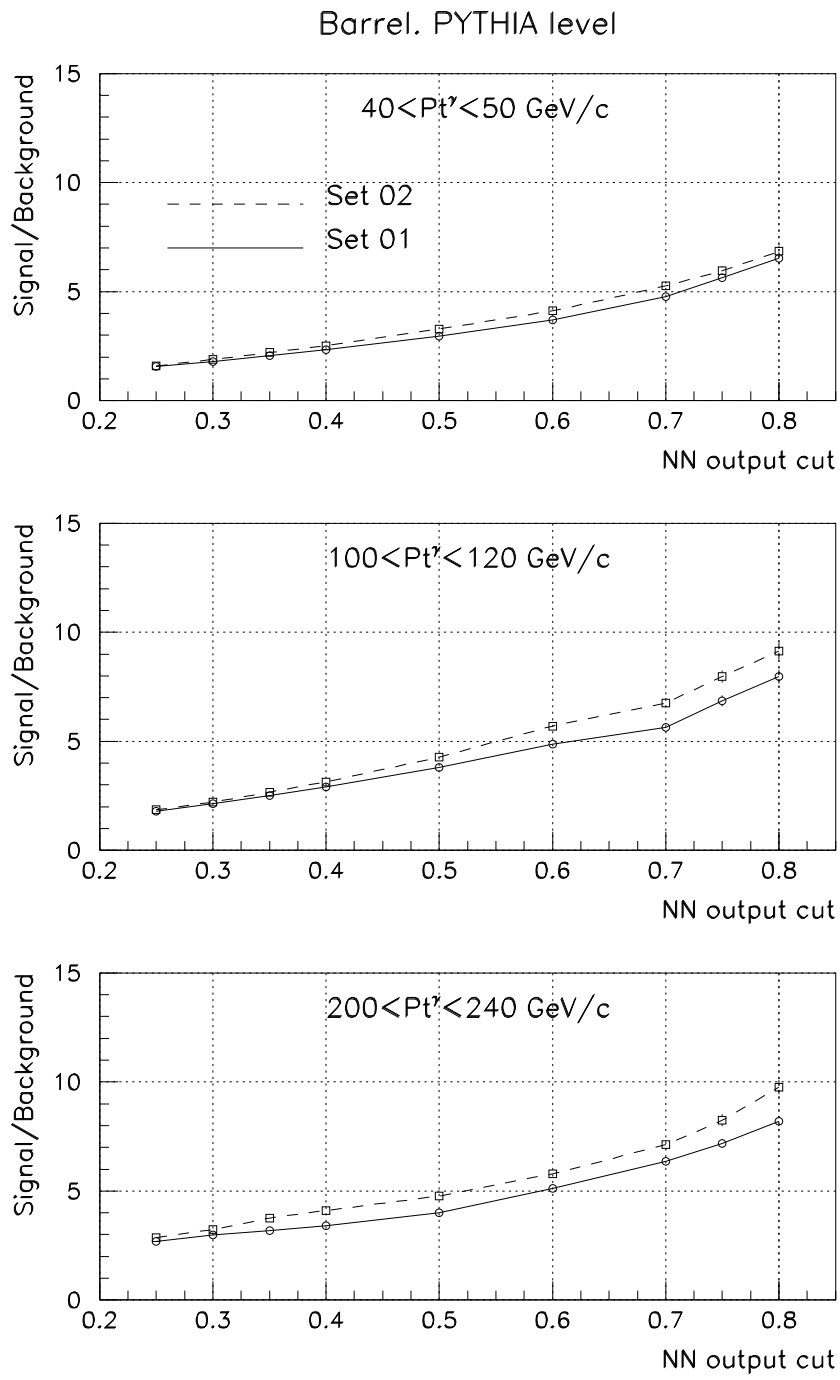


Fig. 12: Signal/Background ratio as a function of separation point at the PYTHIA level. Barrel.

Endcap+Forward. PYTHIA level

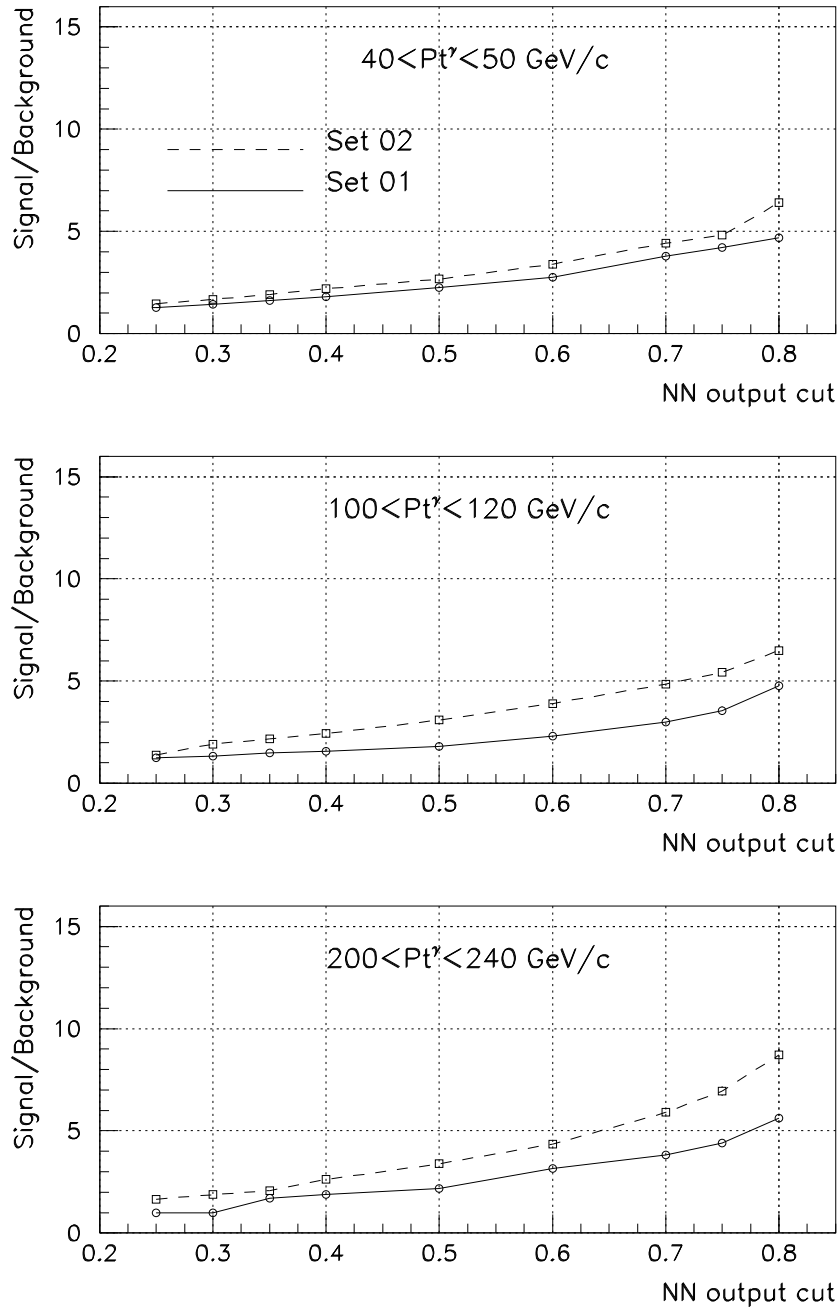


Fig. 13: Signal/Background ratio as a function of separation point at the PYTHIA level. Endcap+Forward